

Revisiting Numerical Simulation of Hot Jet in Cross Flow

Dhanabal K.^a, Nikhil Vijay Shende^{a,*}, Yair Mor-Yossef^b

^a S & I Engineering Solutions Pvt. Ltd., Bangalore 560054, Karnataka, India

^b Israeli CFD Center, Caesarea Industrial Park 3088900, Israel

* Corresponding author email: nikhil.shende.sandi@gmail.com

ABSTRACT

Present study deals with numerical simulation of hot jet in cross flow. The aim of this study is to assess the predictive capability of steady RANS simulations for a complex flow field exhibited by a hot jet issuing in a cross flow. The flow solver employed in the study is HiFUN and the test case is obtained from experimental work of Ramsey and Goldstein. The numerical simulations are carried out on three structured grids of increasing fineness. These grids serve the purpose of carrying out grid independence study. The results presented in this paper bring out the usefulness of steady RANS simulations in predicting temperature distribution for configurations involving hot jet in cross flow. In particular, k- ω SST turbulence model is seen to predict temperature distribution for such configuration both qualitatively and quantitatively with reasonable accuracy required from the view point of engineering analysis.

Keywords: *Jet in cross flow, RANS method, k- ω SST turbulence model, k- ω TNT turbulence model.*

INTRODUCTION

There are number of industrial applications which involve a hot jet issuing normally in cross flow. The exhaust of an industrial chimney, funnel exhaust for ship, vehicle exhausts, injectors for cooling system are some of several practical applications that warrant study of hot jet in cross flow. The complex flow field for this configuration is depicted in Figure 1 [1].

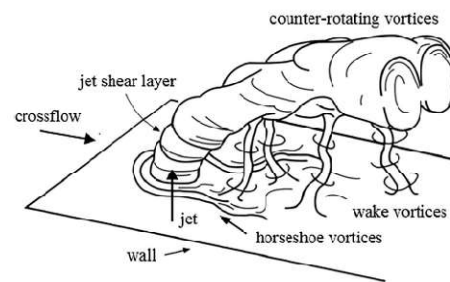


Figure 1: Schematic of jet issuing normal to cross flow and associated flow features [1]

With respect to the cross flow direction and the jet emanating vertically upwards from the injection hole as shown in Figure 1, the flow field around and behind the injection location may be categorized as follows:

1. Jet shear layer vortices in the mixing region just after injection.
2. Horse shoe vortices wrapped around the windward side of the injection hole close to the cross flow boundary layer.
3. Wake vortices underneath the jet plume.
4. Counter rotating vortex pair along the jet trajectory and across the entire jet plume in the region downstream of the injection hole [2].

Owing to this complex flow field, even today, the numerical simulation of hot jet in cross flow is extremely challenging. In the past, numerical studies of jet in cross flow have been carried out with different complexity levels. Direct numerical simulation (DNS) [3], the most appropriate numerical tool to simulate aforementioned flow field with highest fidelity level, is restricted to low Reynolds number flows due to very high computational cost. The use of techniques such as large eddy simulation (LES) [4, 5] and hybrid RANS-LES or detached eddy simulation (DES) [6] are becoming increasingly popular, they still grapple with the penalty of high computational

cost. The problem of computational cost is even more accentuated when hot jet in cross flow becomes a part of larger system such as simulating thermal environment and assessing air pollution due to efflux gases on a ship superstructure with single or multiple funnels. In such a study, the grid size could be well in excess of tens of millions volumes to represent both the geometric complexity and complex flow physics associated with the problem. In this context the present study aims at revising numerical simulation of hot jet in cross flow simulations using steady RANS methodology from an engineering view point. The present study employs the flow solver HiFUN (High Resolution Flow Solver on Unstructured Meshes) [7] for numerical analysis. The test case corresponding to hot jet in cross flow is obtained from the experimental work of Ramsey and Goldstein [8].

THE HiFUN SOLVER

The flow solver HiFUN [7] is an industrial tool based on unstructured data based cell-centre finite volume methodology. It solves unsteady, compressible 3-dimensional (3D) Reynolds Averaged Navier Stokes (RANS) equations. This robust, fast, accurate and efficient tool provides aerodynamic design data in attractive turn-around time. One of the important strengths of the HiFUN solver is its ability to exploit the architecture of CPU based massively parallel supercomputer platforms [9]. To cite an example, HiFUN is capable of providing a complex high lift wing flow solution on a grid with around 150 million volumes employing 15000 Xeon processor cores in less than 30 minutes. The HiFUN solver employs two well known turbulence models, namely, Spalart Allmaras [10] and k- ω SST [11]. In addition, the HiFUN solver employs a relatively less popular turbulence model called k- ω TNT [12]. An advantage of TNT model over SST model is that TNT model does not require calculation of cell distance from nearest wall which makes it attractive for unsteady turbulent simulations involving relative motion of bodies.

TEST CASE SETUP

The test case corresponding to hot jet in cross flow is obtained from the experimental work of Ramsey and Goldstein [8]. The cross flow air velocity is 30 m/s and the blowing ratio, i.e., $(\rho_{jet} V_{jet}) / (\rho_{crossflow} V_{crossflow})$ is 2.0. In the above equation, ρ_{jet} and V_{jet} correspond to density and exit velocity of hot air jet respectively while $\rho_{crossflow}$ and $V_{crossflow}$ correspond to density and velocity of the cold air respectively. The temperature of hot air at jet inlet is 55° C above the cross flow cold air temperature. The hot jet is issued from a 2.35 cm diameter circular opening into the cross stream. The computational domain with various boundary conditions is depicted in Figure 2. The cold air flow is issued into the computational domain in longitudinal direction from boundary patch A (refer Figure 2) via pressure inlet boundary condition. The hot air is issued into the domain from boundary patch E in direction perpendicular to the cold air flow via another pressure inlet boundary

condition. The boundary patch E is circular with the diameter of 2.35 cm. The experimental set up [8] ensures fully developed turbulent pipe flow and uniform temperature distribution at the hot jet exit in the absence of cross flow. The boundary patch D denotes no-slip and adiabatic wall. As given in the experimental set up, the longitudinal distance of viscous wall till the jet inlet is sufficient to grow the boundary layer with displacement thickness of 0.09 cm [8] at cross flow cold air velocity of 30 m/s in the absence of hot jet issuing into the computational domain. It is also given in the experimental work [8] that the boundary layer on the test section is ensured to be fully developed and turbulent by employing boundary layer trip wire. In addition, steady state conditions are ensured during experimental tests [8]. The boundary patch C denotes outlet of the computational domain simulated using a pressure outlet boundary condition. Remaining boundary patches (which include patch B) are set to slip wall boundary condition enforcing no normal flow across these boundary patches. The use of slip wall boundary condition for these patches stems from the fact that boundary layer developed on these surfaces does not play any significant role in altering the flow field in the computational domain. The presence of these boundaries is felt only through modification in pressure field due to lack of fluid penetration through these boundaries. In this paper, the boundaries A, E and C will be referred to as cold flow inlet, hot jet inlet and outlet boundaries respectively.

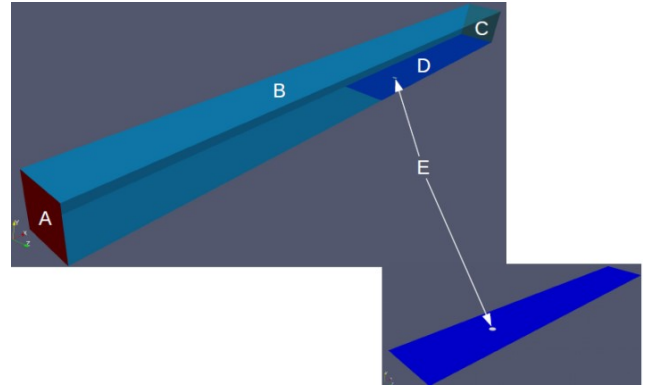


Figure 2: Computational domain with boundaries for hot jet in cross flow simulations

BOUNDARY CONDITIONS

The details pertaining to boundary conditions employed in the present computation are as follows:

- (1) **Cold Flow Inlet:** Velocity = 30.0 m/s, Temperature = 297.15° C, Pressure = 90399 Pa, Turbulence intensity = 0.5%.
- (2) **Hot Jet Inlet:** Velocity = 71.1 m/s (corresponding to blowing ratio of 2.0), Temperature = 352.15° K (which is 55° C above cold air temperature), Pressure = 90399 Pa, Turbulent intensity = 0.5%.
- (3) **Outlet Boundary:** Exit pressure = 90399 Pa.

GRIDS

In present study, grid convergence study is carried out to obtain grid independent solution using three structured grids

having hexahedral elements. The number of volumes in these grids is 4 million, 20 million and 60 million. These grids are referred to coarse, medium and fine respectively. In all three grids, a boundary padding is generated on the viscous wall (boundary patch D in Figure 2) to capture turbulent boundary layer. The first spacing off the viscous wall is chosen such that computed y^+ is less than 1 ensuring at least one cell within viscous sub-layer. The top view of surface grid around the jet inlet (boundary patch E) and mid-section cut plane view for coarse grid are shown in Figure 3.

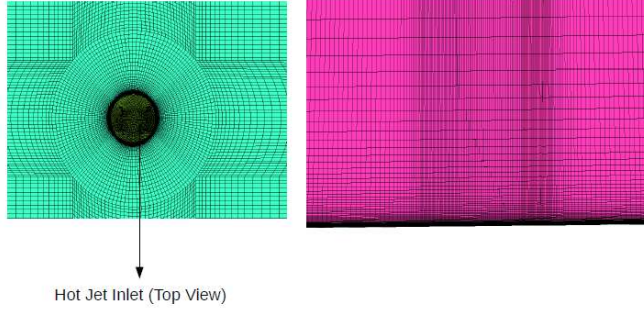


Figure 3: Top view of surface grid around jet inlet and a mid-section view of volume grid

RESULTS AND DISCUSSION

In the present study, steady RANS numerical simulations are performed using k- ω SST and k- ω TNT turbulence models. The inviscid fluxes are computed using Roe [13] scheme. First order backward Euler implicit procedure in conjunction with symmetric Gauss Seidel relaxation procedure [14] is employed for time integration. Weiss and Smith preconditioning [15] method is employed to handle low speed flow encountered in the present simulations.

At the outset, computations are performed on coarse grid. Figure 4 depicts fill plots of temperature distribution on a plane normal to longitudinal direction at a downstream distance of 10.7 times jet inlet diameter. From this figure, it is evident that SST model fails to predict expected symmetry in temperature distribution in the region of counter rotating vortices while TNT model does predict the symmetry in temperature distribution. While the reason for lack of symmetry in the temperature distribution predicted by SST model is not yet clear, a modified version of SST turbulence model [16] also produced results similar to the SST model [11]. This result clearly brings out the efficacy of TNT turbulence model in predicting the temperature distribution for hot jet in cross flow simulations. Therefore only TNT model is considered for the grid convergence study.

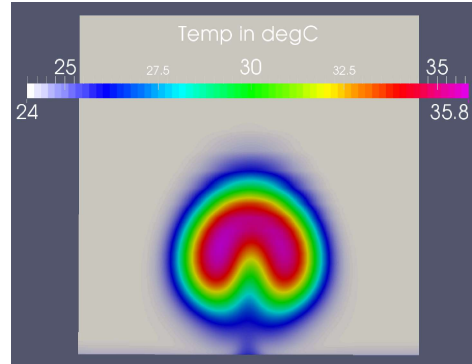
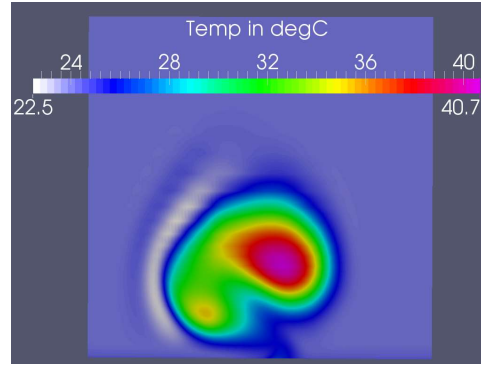


Figure 4: Temperature fill plot on a plane normal to longitudinal direction using SST model (top) and TNT model (bottom) on coarse grid

Figure 5 depicts the relative comparison of temperature distribution on a longitudinal plane passing through the center line of the jet inlet using TNT turbulence model. From this figure it may be seen that the flow features become sharper on medium grid compared to coarse grid while those between medium and fine grid do not show appreciable difference.

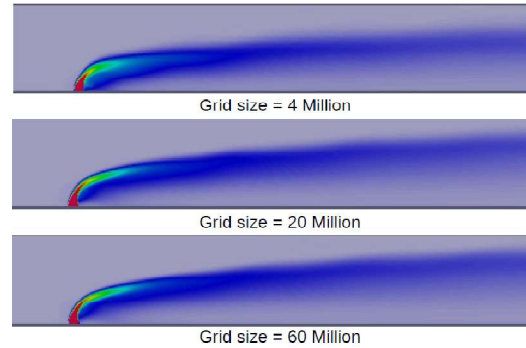


Figure 5: Temperature fill plots obtained using TNT model on coarse (4 Million), medium (20 Million) and fine (60 Million) grids

Figure 6 depicts fill plot of normalized temperature distribution on planes normal to longitudinal direction at a downstream distance of 1.37 and 10.7 times jet inlet diameter. The normalized temperature is defined as the ratio of difference in temperatures at a point and cold flow inlet to the difference in temperatures at hot jet inlet and cold flow inlet. From this figures too, it may be seen that the flow features become sharper on medium grid compared to coarse grid while those between medium and fine grid do not show appreciable difference.

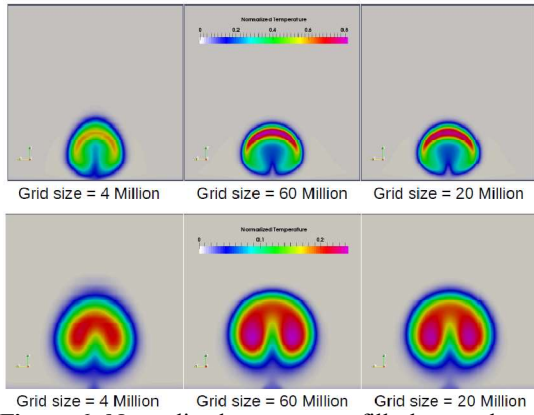


Figure 6: Normalized temperature fill plot on planes normal to longitudinal direction at downstream distance of 1.37 (top) & 10.07 (bottom) times jet inlet diameter using TNT model on coarse (4 Million), medium (20 Million) and fine (60 Million) grids

Figure 7 depicts the comparison of normalized temperature distribution between experimental and numerical results along vertical lines drawn on longitudinal plane passing through center line of the jet inlet. All these vertical lines start from the wall. These lines are drawn at longitudinal (i.e. in the direction of cross flow) locations 1.37 and 10.07 times jet inlet diameter downstream of the jet entry. In this figure, the legends TNT, TNT Medium and TNT Fine stand for results on coarse, medium and fine grids respectively. From these line plots, it may be clearly seen that numerical predictions on medium and fine grids show lower spread of hot jet compared to that on coarse grid as the jet evolves in downstream direction. Further medium and fine grids show higher temperature values in jet core close to jet inlet indicating lower mixing of hot and cold streams compared to experimental results. Also, numerical results show higher elevation of maximum temperature location from wall compared to experimental results.

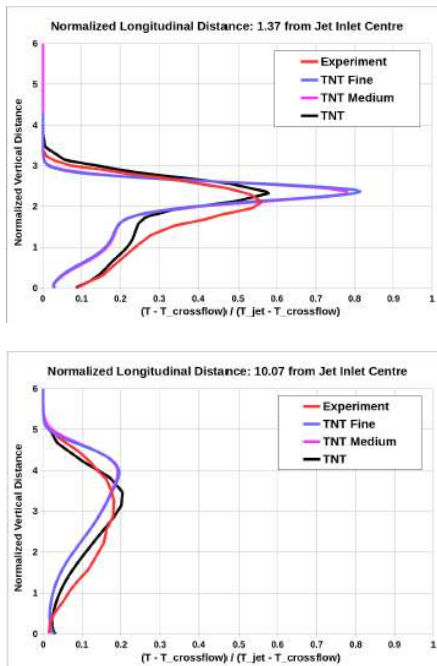


Figure 7: Comparison of normalized temperature

distribution at locations having downstream distance of 1.37 and 10.07 times jet inlet diameter

Figure 8 depicts the comparison of normalized velocity distribution between experimental and numerical results along vertical lines drawn on longitudinal plane passing through center line of the jet inlet. The velocity is normalized using cold air flow velocity, i.e., 30 m/s. From these line plots it may be seen that numerical simulations show steeper velocity gradients compared to experimental results. Also, the location of maximum velocity point from wall predicted using numerical computations is close to that predicted in the experiment.

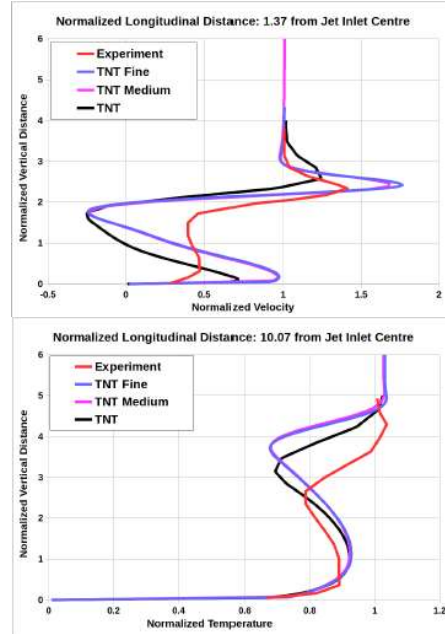


Figure 8: Comparison of normalized velocity distribution at locations having downstream distance of 1.37 and 10.07 times jet inlet diameter

Figures 9 and 10 depict lines corresponding to maximum temperature and velocity locations respectively on longitudinal plane passing through jet center line. From Figure 9, it may be seen that the location of maximum temperature predicted by numerical simulation on coarse grid compares well with experimental data while that predicted by numerical simulations on medium and fine grids is higher than the experimental location. On the contrary, the location of maximum velocity predicted by numerical simulations on all the grids (refer to figure 10) is in close agreement with one another and experimental results.

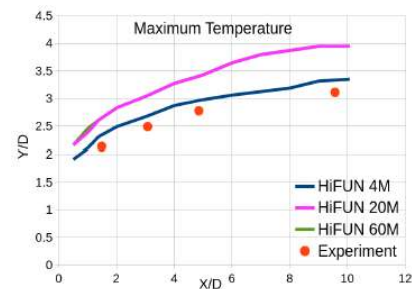


Figure 9: Line depicting maximum temperature location on longitudinal plane passing through jet centreline

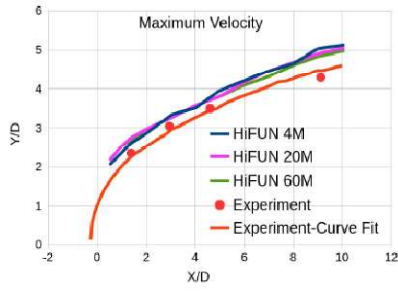


Figure 10: Line depicting maximum velocity location on longitudinal plane passing through jet centreline

Since the numerical results obtained on medium and fine grids are very close to one another (refer figures 5 to 10), it may be concluded that grid converged solution is obtained on medium grid itself.

Figures 11-(top) and 12-(top) depict the comparison of normalized temperature contours on a plane normal to longitudinal direction at downstream distances of 1.37 and 4.96 times the jet inlet diameter on coarse grid obtained using numerical simulation and experiment. The numerals shown in the legends of these figures depict normalized temperature values for which the contours are drawn. From these figures, it may be seen that normal and lateral spread of the jet at longitudinal locations considered in these figures (as seen from contour line corresponding to normalized temperature value of 0.1) are predicted well by the numerical simulation on coarse grid. Further as we move inward towards hot core of the jet, the numerical contours show an upward shift compared to experimental contours. Also the numerical simulation predicts steeper temperature gradients around jet centreline closer to the wall (i.e. between the regions $Z/D = 0$ and $Z/D = \pm 0.015$; $Y/D = 0$ corresponds to wall) compared to experimental results.

Figures 11-(bottom) and 12-(bottom) depict the comparison of normalized temperature contours on a plane normal to longitudinal direction at downstream distances of 1.37 and 4.96 times the jet inlet diameter on fine grid obtained using numerical simulation and experiment. From these figures, it may be seen that normal and lateral spread of the jet at longitudinal locations considered in these figures (as seen from the contour line corresponding to normalized temperature value of 0.1) are predicted well by the numerical simulation on fine grid. Further, similar to coarse grid results, as we move inward towards hot core of the jet, the numerical contours show an upward shift compared to experimental contours. This observation corroborates with the results presented in Figure 9 which show lines of maximum temperature location predicted on medium and fine grids above the experimental location. The numerical simulation also predicts much steeper temperature gradients around jet centreline closer to the wall (i.e. between the regions $Z/D = 0$ and $Z/D = \pm 0.015$; $Y/D = 0$ corresponds to wall) compared to experimental results. At this stage it should be remarked that the normalized temperature contours obtained on medium grid match very closely with the fine grid and hence are not presented here.

The reason for discrepancy in temperature prediction as seen in Figures 7, 9, 11 and 12 may be attributed to the assumption of constant turbulent Prandtl number for this type of flows. As in standard turbulence modelling practice, numerical simulations in present study employ a constant turbulent number of 0.9 to calculate eddy thermal diffusivity from eddy viscosity. However as shown in experimental work by Andreopoulos [17], turbulent Prandtl number varies in direction normal to wall: closer to wall it has rather high values (> 1) and reaches values around 0.9 away from wall.

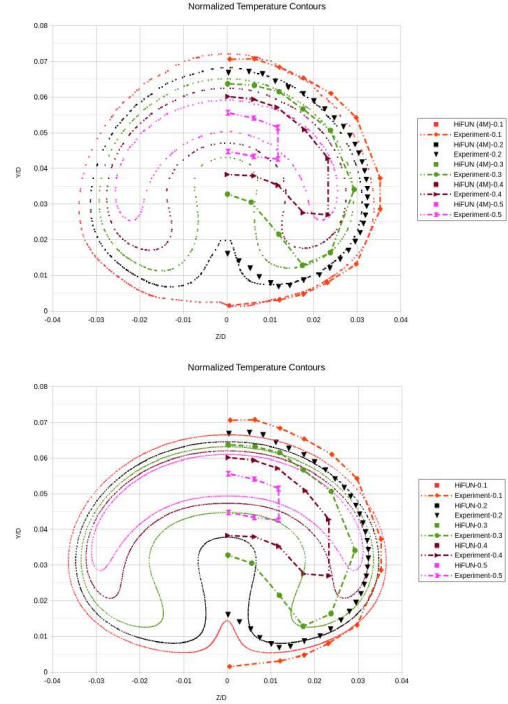


Figure 11: Normalized temperature contours on plane normal to longitudinal direction at downstream distance 1.37 times jet inlet diameter on coarse (top) and fine (bottom) grid

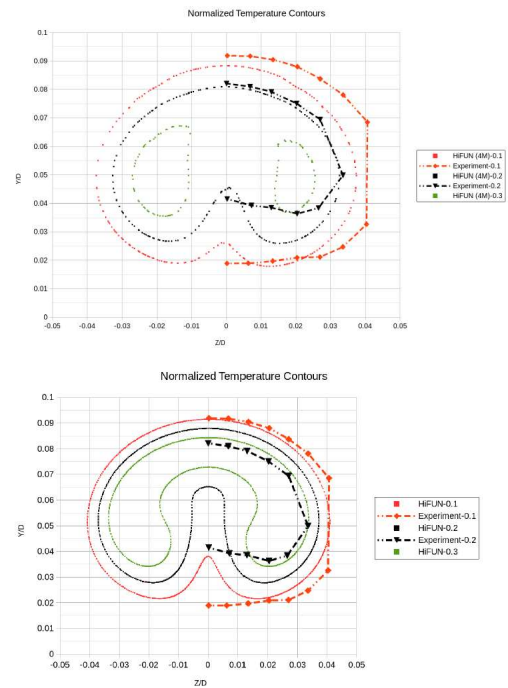


Figure 12: Normalized temperature contours on plane normal to longitudinal direction at downstream distance 4.96 times jet inlet diameter on coarse (top) & fine (bottom) grid

CONCLUSIONS AND FUTURE DIRECTION

The aim of present study is to assess predictive capability of steady RANS simulations for a complex flow field exhibited by a hot jet issuing in a cross flow. The flow solver employed in the study is HiFUN. The test case corresponding to hot jet in cross flow is obtained from experimental work of Ramsey and Goldstein. The numerical simulations are carried out on three structured grids of increasing fineness. The important conclusions of this study are as follows: (1) k- ω SST turbulence model fails to predict symmetry in temperature distribution while TNT model does predict symmetry in temperature distribution in the regions of counter rotating vortices. (2) Since numerical results obtained on medium and fine grids using TNT model are very close to one another, it may be said that grid converged solution for the present test case is obtained on medium grid itself. (3) While the location of maximum temperature in longitudinal direction on center plane of jet predicted by numerical simulation on coarse grid compares well with experimental data, that predicted by numerical simulations on medium and fine grids is higher than experimental location. (4) The location of maximum velocity in longitudinal direction on center plane of jet predicted by numerical simulations on all the grids is in close agreement with one another and experimental results. (5) As the jet evolves in longitudinal direction, its normal and lateral spread is predicted well by numerical simulations. (6) The numerical simulations predict steeper temperature gradients around jet centreline closer to the wall compared to experimental results. (7) The discrepancy in temperature prediction between numerical and experimental results may be attributed to the assumption of constant turbulent Prandtl number in numerical computations for this type of flows since experiment show that turbulent Prandtl number significantly vary in the direction normal to wall.

In summary, this work brings out usefulness of steady RANS simulations in predicting temperature distribution for configurations involving hot jet in cross flow. In particular, k- ω TNT turbulence model is seen to predict the temperature distribution for such configuration both qualitatively and quantitatively with reasonable accuracy required from the view point of engineering analysis. As way forward, authors plan to consider turbulence models which either directly model eddy thermal diffusivity [18] or turbulent Prandtl number [19]. In addition, scale adaptive turbulent simulation [20] and detached eddy simulations (DES) [6] will also be explored. Even though DES is computationally much more expensive than steady RANS simulation, new generation computer hardware such as NVIDIA GPU based accelerator augmenting computing power of traditional CPU based computer is showing lot of promise in bringing down computing turnaround time to acceptable limit.

References

1. Fric, T. F., and Roshko, A., "Vortical Structure in the Wake of a Transverse Jet," *J. Fluid Mech.*, 279, pp. 1–47, 1994.
2. Liwei Zhang and Vigor Yang, "Flow Dynamics and Mixing of a Transverse Jet in Crossflow Part I: Steady Crossflow", *Journal of Engineering for Gas Turbines and Power*, Vol. 139, August 2017.
3. Muppidi, S., and Mahesh, K., "Study of Trajectories of Jets in Crossflow Using Direct Numerical Simulations," *J. Fluid Mech.*, 530, pp 81-100, 2005.
4. Jones, W. P., and Wille, M., "Large-Eddy Simulation of a Plane Jet in a Cross-Flow," *Int. J. Heat Fluid Flow*, 17(3), pp. 296–306, 1996.
5. Yuan, L. L., Street, R. L., and Ferziger, J. H., "Large-Eddy Simulations of a Round Jet in Crossflow," *J. Fluid Mech.*, 379, pp. 71–104, 1999.
6. Simone Camarri, Vanessa Mariotti, Maria Vittoria Salvetti, Bruno Koobus, Alain Dervieux, Hervé Guillard, Stephen Wornom, "Numerical simulation of a jet in crossflow. Application to GRID computing", Research Report RR-5638, INRIA, pp. 80, 2006.
7. <http://www.sandi.co.in/home/products> Last accessed on 15th June 2019.
8. J. W. Ramsey and R. J. Goldstein, "Interaction of a heated jet with a deflecting stream", NASA CR-72613, April 1970.
9. <http://www.sandi.co.in/v2/home/hifun1.pdf> Last accessed on 15th June 2019.
10. Spalart P. R. and Allmaras S. R., "A One-Equation Turbulence Model for Aerodynamic Flows", AIAA Paper 92-0439, 1992.
11. Menter, F. R., "Two-Equation Eddy-Viscosity Turbulence Models for Engineering Applications", AIAA Journal, Vol. 32, No. 8, August 1994, pp. 1598-1605.
12. C. Kok, Johan, "Resolving the dependence on freestream values for the k- ω turbulence model", AIAA Journal, Vol. 38, No. 7, 2000, pp. 1292–1295.
13. Roe Philip L., "Approximate Reimann Solvers, Parameter Vectors and Difference Schemes", *Journal of Computational Physics*, Volume 43, Issue 2, pp. 377-372, October 1981.
14. Shende Nikhil and Balakrishnan N., "New Migratory Memory Algorithm for Implicit Finite Volume Solvers", AIAA Journal, Vol. 42, No. 9, September 2004, pp. 1863-1870.
15. Jonathan M. Weiss and Wayne A. Smith, "Preconditioning Applied to Variable and Constant Density Flows", AIAA Journal, Vol. 33, No. 11, November 1995.
16. Menter, F. R., Kuntz, M., and Langtry, R., "Ten Years of Industrial Experience with the SST Turbulence Model", *Turbulence, Heat and Mass Transfer 4*, ed: K. Hanjalic, Y. Nagano, and M. Tummers, Begell House, Inc., 2003, pp. 625-632.
17. J. Andreopoulos, "Heat Transfer Measurements in a Heated Jet-Pipe Flow Issuing into a Cold Stream", *The Physics of Fluids*, Vol. 26, No. 11, pp. 3201-3201, November 1983.
18. Elizaveta Ivanova, Berthold Noll, Massimiliano Di Domenico and Manfred Aigner, "Improvement and Assessment of RANS Scalar Transport Models for Jets in Crossflow", AIAA Paper 2008-565, January 2008.
19. Jonas Bredberg, Shia-Hui Peng and Lars Davidson, "An improved k- ω turbulence model applied to recirculating flows", *International Journal of Heat and Fluid Flow*, Vol. 23, pp. 731-743, 2002.
20. Benjamin M. Duda, Florian R. Menter, Sébastien Deck, Hervé Bézard, Thorsten Hansen and Marie-Josephe Estève, "Application of the Scale-Adaptive Simulation to a Hot Jet in Cross Flow", AIAA Journal, Vol. 51, No. 3, pp. 674-684, March 2013.